Translational

Monitoring Morphological Changes in the Retina of Rhodopsin$^{-/-}$ Mice with Spectral Domain Optical Coherence Tomography

Ruilin Wang,[1,2] *Caihui Jiang,*[2] *Jie Ma,*[2] *and Michael J. Young*[2]

Purpose. The rhodopsin$^{-/-}$ C57Bl/6 (rho$^{-/-}$) mouse is a very important model for understanding retinal degenerative diseases. In this study, spectral domain optical coherence tomography (SD-OCT) was used to monitor the dynamic morphological changes in retina of rho$^{-/-}$ mice.

Methods. Rho$^{-/-}$ mice and wild type C57Bl/6 (B6) mice at the age of 3, 6, 9, and 12 weeks were investigated using SD-OCT to obtain cross-sectional images of the retina. The outer nuclear layer (ONL) thickness was measured. Histological sections were used to compare to the OCT data. Electroretinograms (ERG) were performed to evaluate the physiological change for establishing the relationship between retinal morphology and its functional changes.

Results. There was no apparent morphological or functional change in B6 mice at any time point. The SD-OCT measurement showed that the ONL thickness in rho$^{-/-}$ mice was significantly decreased from 40.6 μm to 6.0 μm from week 3 to week 12 postnatal. Histological examinations identified a similar trend, although the average thickness of ONL from histological sections at these time points was slightly larger (ranging from 55.4 μm to 14.9 μm). The ERG in rho$^{-/-}$ mice indicated functional changes that were in concordant with morphological changes; a significant linear positive association was identified between the amplitude of b-wave and the ONL thickness.

Conclusions. Our findings confirmed that the functional changes in retina were concordant with morphological changes measured by SD-OCT in vivo, which indicates that SD-OCT can be used as a reliable noninvasive method to monitor the degenerative progression in retinal disease models. (*Invest Ophthalmol Vis Sci.* 2012;53:3967–3972) DOI: 10.1167/iovs.12-9716

Retinitis pigmentosa and age-related macular degeneration (AMD) are two major retinal degenerative diseases that cause irreversible blindness.[1–3] Rodent models are very important tools for understanding these diseases, including the process and mechanism of degeneration, and also very valuable in developing treatment methods.

Previous studies showed that rhodopsin is an essential element in photo-transduction and a structural protein in rod outer segment.[4,5] In this study, rho$^{-/-}$ mice were used because their degeneration has been well characterized; rho$^{-/-}$ mice do not express rhodopsin, and therefore, do not form rod outer segments (ROS). Specifically, the nonfunctional rods slowly degenerate over a period of months, followed by the loss of cone photoreceptors.[6–8] Therefore, this model offers the opportunity to explore regenerative therapies that replace rods, as well as those that preserve the life of cones. These avenues of intervention can be explored morphologically and functionally.

Animals have to be sacrificed at different time points for conventional anatomical investigation in the studies of degenerative diseases; each animal only provides a single time point in the degenerative progression. Those studies usually require a large number of animals to yield reliable conclusions. A noninvasive examination, which can monitor the disease progression, is preferable. Both ultrasonography and OCT can be used noninvasively in clinical examinations. Compared with OCT, ultrasonography has certain limitations, such as coupling agent requirement and poor resolution. Even high frequency ultrasound (50–100 mHz) is unable to provide high-resolution histological-like images such as can be provided by OCT.[9]

Here, study authors provide a noninvasive in vivo assessment of the outer nuclear layer (ONL) thickness (an indicator of photoreceptor survival) by SD-OCT, and evaluate the assessment by comparing the associative dynamic changes between morphological measurements and functional evaluation by ERG. These results not only allow dynamic monitoring of retinal progressive degeneration, but also provide the basis for future studies on the diagnosis and treatment of the retinal diseases.

Materials and Methods

Animals

Rho$^{-/-}$ mice (Peter Humphries, Trinity College, Dublin) and B6 mice (Jackson Laboratory, Bar Harbor, ME) at the age of 3, 6, 9, and 12 weeks were used in this study. Each type of mouse was divided into three groups for different examinations (SD-OCT, ERG, and histology). Seven mice of each type were used to perform SD-OCT and ERG examinations. These mice were tested at four time points. For the histological investigation, there were two rho$^{-/-}$ mice sacrificed at each time point, and B6 mice at the age of 3 weeks and 9 weeks were used (two mice for each time point) for comparison. All experiments were performed in compliance with the ARVO Statement for the Use of

From the [1]Department of Ophthalmology, Tongji Hospital, Tongji Medical School, Huazhong University of Science and Technology, Wuhan, China; and the [2]Schepens Eye Research Institute, Massachusetts Eye and Ear Infirmary, Department of Ophthalmology, Harvard Medical School, Boston, Massachusetts.

Supported by grants from Reneuron Group plc, Charles de Gunzburg Foundation, and Grousbeck Foundation.

Submitted for publication February 16, 2012; revised May 4, 2012; accepted May 13, 2012.

Disclosure: **R. Wang**, None; **C. Jiang**, None; **J. Ma**, None; **M.J. Young**, None

Corresponding author: Michael J. Young, Schepens Eye Research Institute, Massachusetts Eye and Ear Infirmary, Department of Ophthalmology, Harvard Medical School, 20 Staniford Street, Boston, MA 02114; michael.young@schepens.harvard.edu.

Animals in Ophthalmic and Vision Research and the Schepens Eye Research Institute Animal Care and Use Committee.

SD-OCT Imaging

SD-OCT was performed using the ophthalmic imaging system (Bioptigen Spectral Domain Ophthalmic Imaging System; Bioptigen, Inc., Durham, NC). The system has a probe and a platform designed for mice that can easily orient and align the subject. Animals were anesthetized by intraperitoneal injection with a solution of ketamine (120 mg/kg) and xylazine (20 mg/kg). Pupils were dilated using 1% tropicamide (Akorn, Lake Forest, IL). Lubricant gel drops (Novartis Pharmaceuticals Corp, East Hanover, NJ) were applied to the animal eyes every 3 minutes to prevent cornea dehydration.

Imaging and data process were performed with image analysis software (InVivoVue Clinic; Bioptigen). Briefly, radial volume scan (centered on optic disc, diameter 1.3 mm) was used, each volume consisting of 100 B-scans (1,000 A-scans per B-scan). Four scans (scan 1, 26, 51, and 76 at 0°, 45°, 90°, and 135° in en-face image) were selected for the ONL thickness measurement. Four vertical calipers (defining the ONL, from the outer plexiform layer [OPL] to the outer limiting membrane [OLM]) were placed on each scan, with two on each side of the optic disc, 250 μm and 500 μm away from the optic disc, respectively.

Histological Examination

Animals were euthanized with CO_2 at the selected time points. Eyeballs were enucleated and fixed in 10% formalin 48 hours prior to dehydration and casted in rapid polymerizing methyl methacrylate (Technovit 7100; VWR, West Chester, PA). Samples were removed, mounted on microtome chucks, and vertical semi-thin sections were cut through the center of the eye. H&E staining was performed using standard protocols. Four images (60× magnification) were taken 250 μm and 500 μm from the optic disc (two on each side) for each sample (Nikon Eclipse E800; Nikon, Tokyo, Japan). Five vertical lines were randomly drawn between the outer plexiform layer and outer limiting membrane on each image. The length of the line was measured as the thickness of the ONL. The number of nuclei touching the line was also counted as the number of nuclei in the ONL.

ERG Recording

Animals were dark adapted for at least 6 hours prior to ERG recording. All the procedures were performed in a dark room with a dim red safety light. Animals were anesthetized by intraperitoneal injection with a solution of ketamine (120 mg/kg) and xylazine (20 mg/kg). Pupils were dilated using 1% tropicamide. Animals were placed in a sternal-abdominal position within the Ganzfield bowl. Body temperature was maintained at 37°C by heating pad to prevent hypothermia. Two active gold lens electrodes were placed on each cornea. The reference and ground electrodes were placed subcutaneously in the midfrontal area of the head and the back area near to the tail, respectively. Light stimulations were delivered with a xenon lamp at 3.0 cd·s/m^2 for the dark-adapted test and 10.0 cd·s/m^2 for the light-adapted test. The animals were subjected to the light adaptation for 10 minutes, and the intensity of the background light was 30 cd s/m^2. The data were recorded and processed by the software included with the ERG machine (Espion Electroretinography System; Diagnosys LLC, Lowell, MA). The a-waves were measured from the baseline to the cornea-negative peak, and b-waves were measured from the cornea-negative peak to the major cornea-positive peak.

Statistical Analysis

One-way ANOVA was used to compare the difference among groups using the software of SPSS 19.0. Correlation between the morphological and functional measurements was assessed by Pearson's correlation coefficient. Results are presented as mean ± SD and the significant level was set at 0.05.

Results

Examinations using SD-OCT and histology were performed in B6 mice to obtain cross-sectional images representing the different layers of retina (Fig. 1).

OCT Images of Rho$^{-/-}$ and B6 Mice

The ONL thickness of rho$^{-/-}$ mice decreased gradually from week 3 to week 12 postnatal. Significant differences were found among the average thicknesses at each time point (40.6 ± 1.61 μm, 27.9 ± 1.65 μm, 14.5 ± 0.7 μm, and 6.0 ± 0.78 μm, respectively) (One-way ANOVA, $F = 585.83$, $df = 3$, $P < 0.05$). The ONL thickness of B6 mice was constant throughout this period, the average thickness being 52.5 ± 0.69 μm. The SD-OCT images show complete absence of the inner segment/outer segment (IS/OS) junction in rho$^{-/-}$ mice compared with B6 mice at all time points. In the images of B6 mice, there were two clear white layers (OLM; IS/OS, junction between the inner and outer segment of the photoreceptors) beneath the ONL (Fig. 2). However, there was only one layer (outer limiting membrane) beneath the ONL in rho$^{-/-}$ mice (Fig. 2).

Comparing SD-OCT Images with Histology

From the histological sections, the ONL thickness was measured and the ONL nuclei were counted. At week 3, rho$^{-/-}$ mice had 9–10 nuclei in the ONL while B6 mice had 11–

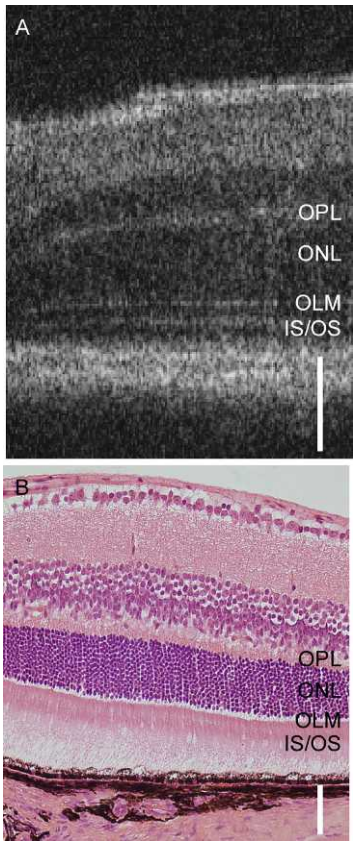

Figure 1. The ONL thickness of B6 mice. (**A**) Measured with OCT imaging system. (**B**) Histological examination. The scale bar in both figures is 50 μm.

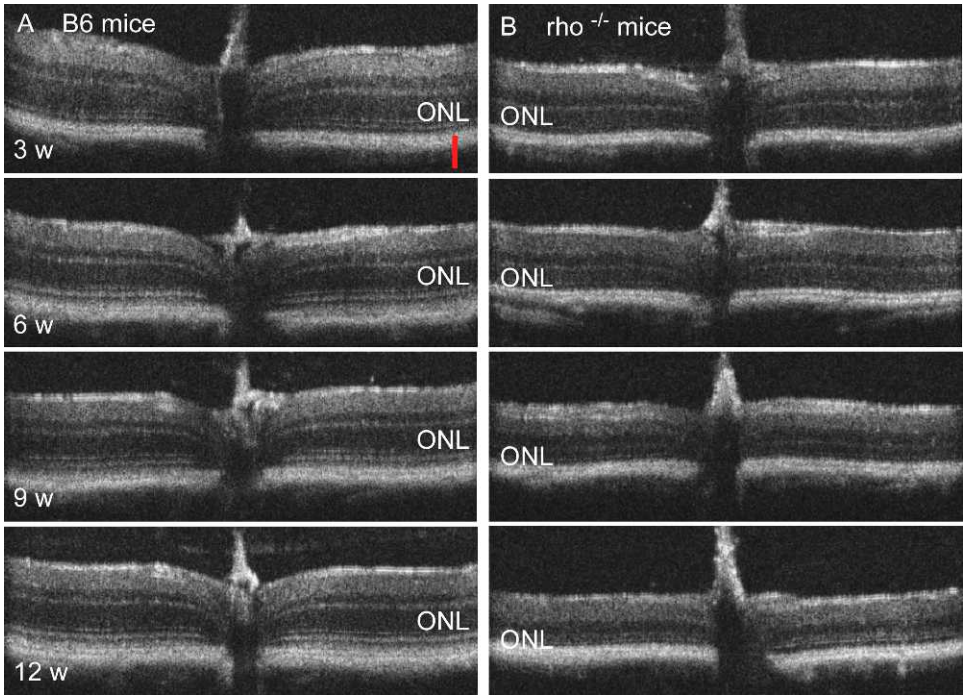

Figure 2. The cross-sectional OCT images. The thickness of ONL in B6 mice was quite stable from week 3 to week 12 (*column A*), but it gradually shrunk to a very thin layer in rho$^{-/-}$ mice (*column B*). The scale bar is 50 μm.

12 nuclei. At week 6, the rho$^{-/-}$ mice had 5–6 nuclei in the ONL. At week 9, the number of nuclei in rho$^{-/-}$ mice was 2–4. At week 12, the number was only 1–2 (Fig. 3). The ONL thickness of rho$^{-/-}$ mice also decreased gradually from week 3 to week 12 (Figs. 3, 4); the thickness was 55.4 ± 3.25 μm, 36.6 ± 2.4 μm, 21.1 ± 2.67 μm, and 14.9 ± 2.18 μm. There were significant differences between these results (One-way ANOVA, $df = 3$, $F = 925.36$, $P < 0.05$). The measurements from SD-OCT and histology of rho$^{-/-}$ mice showed a similar decreasing trend (Fig. 6). No difference was found between the ONL thickness of 3-week and 9-week-old B6 mice (Fig. 4).

ERG Recording

In B6 mice, the waveform pattern and amplitudes (approximately 680 μV) were quite similar to the dark-adapted 3.0 ERG recording from week 3 to week 12 (Fig. 5A). There was no distinct a-wave at any time point for the dark-adapted 3.0 ERG in rho$^{-/-}$ mice. The amplitude of the b-wave decreased gradually from week 3 to week 9 postnatal. The average b-wave amplitudes in rho$^{-/-}$ mice decreased from 196.8 μV to 118.3 μV. At week 12, the b-wave amplitude dropped dramatically to 40.6 ± 23.6 μV in rho$^{-/-}$ mice (Figs. 5A, 5C).

In the light-adapted ERG, there was a stable b-wave with amplitude approximately 120 μV in B6 mice (*left panel*, Fig. 5B). In rho$^{-/-}$ mice, there was no a-wave at any time point. The waveform pattern was similar at week 3 and week 6. The average b-wave amplitudes were 162.8 ± 22.4 μV and 147.6 ± 20.6 μV. At week 9, the b-wave amplitude was reduced by nearly half from week 3 (86.5 ± 16.8 μV). The amplitude of ERG became barely measurable at week 12 (Figs. 5B, 5D).

Association between Morphological and Functional Measurements

A significant positive association was established between the thickness of ONL (measured from SD-OCT images and histological sections) and the amplitudes of b-wave in ERG. When the quantified morphological measurements and functional recordings were applied to $\log_{10}$-transformation, study authors found a linear association between the thickness of ONL and the amplitude of either dark-adapted or light-adapted ERG b-wave of B6 and rho$^{-/-}$ mice. The two linear lines in these two ERG patterns showed the same trend. The ONL thickness became thinner and the ERG amplitudes became smaller (Figs. 6A, 6B). In addition, the measurements from SD-OCT showed more significant linear correlation with ERG b-wave ($R^2 = 0.95$ for dark-adapted 3.0 ERG, $R^2 = 0.94$ for light-adapted 10.0 ERG) than that between histological measurement and ERG b-wave ($R^2 = 0.81$ for dark-adapted 3.0 ERG, $R^2 = 0.80$ for light-adapted 10.0 ERG).

Discussion

Retinitis pigmentosa and age-related macular degeneration all have abnormalities of the photoreceptors of the retina, which lead to progressive visual loss. One area of research that offers promise is cell transplantation to replace or rescue those nonfunctional and dying cells in degenerative retina.[10–13] The total loss of rod function in rho$^{-/-}$ mouse, together with the progressive loss of cones (first functionally and then anatomically), makes it as a suitable platform to evaluate rod replacement and cone rescue function. One major concern is the evaluation of the morphological and functional changes after these interventions. The most common method is to sacrifice the experimental animals and conduct histological examinations. However, this ex-vivo approach has certain limitations, such as variable alterations due to tissue swelling and autolysis after death or tissue shrinkage caused by fixation and dehydration procedures. And even the steps of embedding, staining, cutting, and mounting can cause potential artifacts.[14] Meanwhile, the ex-vivo method is not suitable for evaluating longitudinal dynamic change observation in individual animals. A noninvasive and reliable means for evaluation is desirable.

OCT is a technique based on Michelson interferometry, using low coherence infrared light to obtain cross-sectional or three-

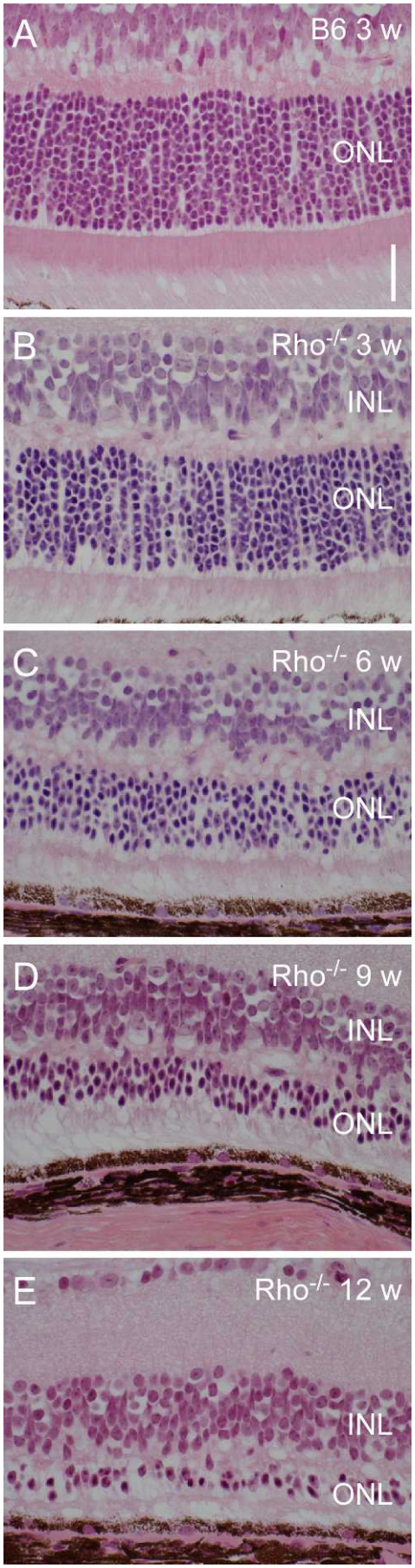

Figure 3. The thickness of ONL in B6 (**A**) was thicker than rho$^{-/-}$ mice and (**B–E**) presented the dynamic morphological change in ONL thickness of rho$^{-/-}$ postnatal from week 3 to week 12. The scale bar is 50 μm.

dimensional images.[15] The transparent feature of the ocular media has made OCT as one of the most developed techniques in the field of ophthalmology.[16–19] Since its first applications,[20–22] OCT has evolved into an ultrahigh resolution, high-acquisition speed, and sensitivity diagnostic tool. Presently, OCT is not only very important in clinic, but also a very valuable tool in ophthalmic research. OCT has been used in many studies to monitor the progress of degeneration in certain types of retinal degenerative mice.[14,23–26] Rho$^{-/-}$ mice are widely used to study the retina degeneration and other therapies; therefore, it is important to characterize this mouse and set up a comparison baseline for these interventions. One primary goal of this study was to assess noninvasively using high resolution SD-OCT to measure the thickness of the ONL in rho$^{-/-}$ mice over a period of time suitable to evaluate interventional strategies, with an aim of providing a background upon which changes in retinal structure and function could be evaluated. Based on available data, this is the first longitudinal study using SD-OCT to monitor the degeneration in rho$^{-/-}$ mice.

Previous work has skillfully described ERG and histological examination of the rho$^{-/-}$ mouse.[6,7] Although the colony of rho$^{-/-}$ mice tested here was obtained almost 9 years ago, no notable differences in results were found in either the morphological or functional level. The dark-adapted 3.0 ERG is typically a quantification of both rod and cone function,[27] although in rho$^{-/-}$ mice one observes only the cone response. This response was already greatly diminished at 3 weeks postnatal compared with the same age B6 mice, with another significant decrease at 9 weeks. These indicate a loss of cone function, which is occurring in the absence of frank cone cell death. These findings are concordant with morphological changes obtained by OCT and histological examination. This further suggests that a decrease in cone function, perhaps mediated through changes in the inner/outer segment region, precedes the death of these cells. A shift in this decreased response to an older age would indicate rescue of cone function and viability. The light-adapted 10.0 ERG is a

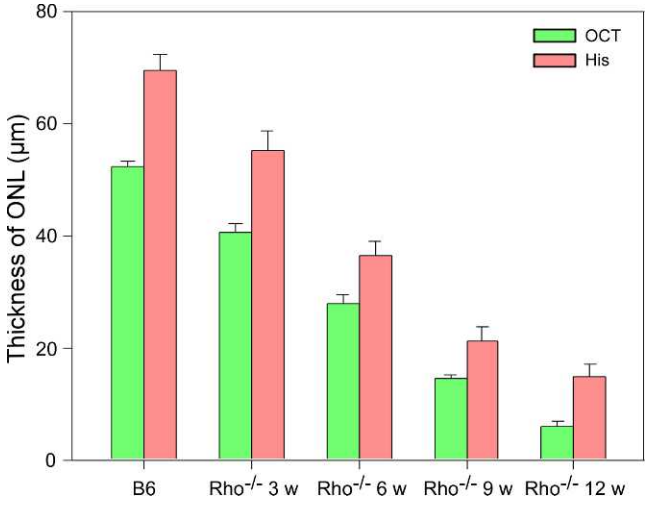

Figure 4. The thickness of ONL from OCT measurements and histological examinations. The ONL gradually shrunk from relatively normal thickness to a thin layer in a few months in rho$^{-/-}$ mice. The ONL in B6 mice (*left two bars*) was relatively thicker than rho$^{-/-}$ mice.

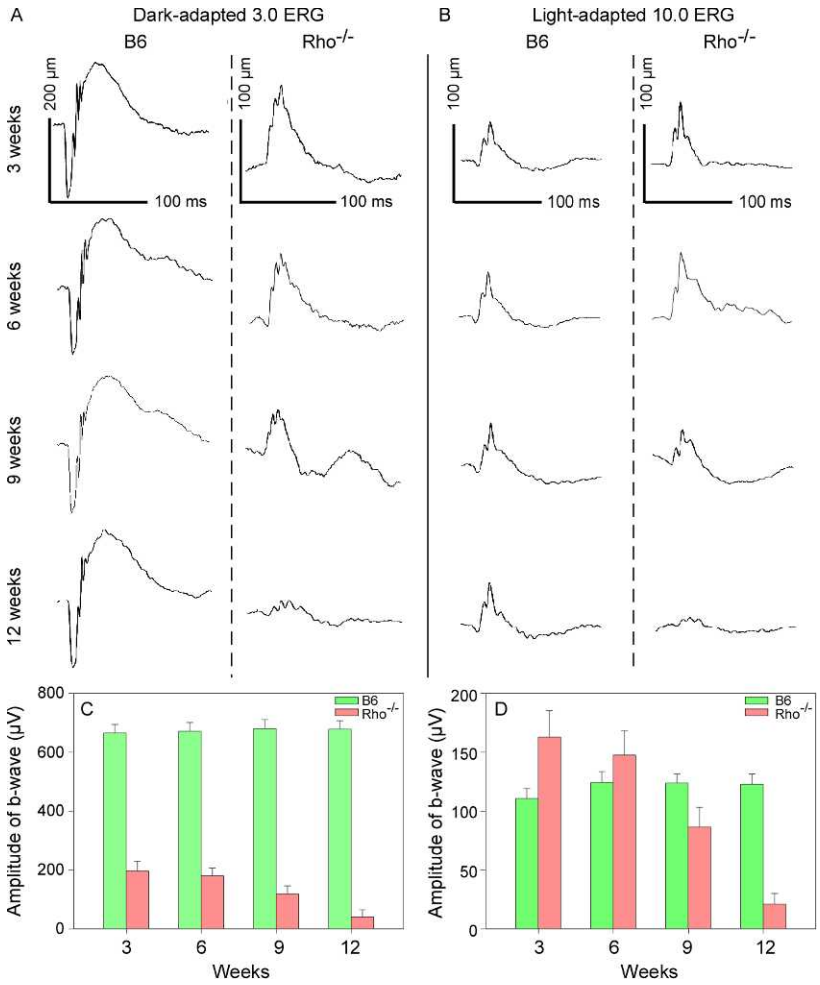

Figure 5. The ERG recordings from B6 and rho$^{-/-}$ mice at dark-adapted and light-adapted conditions from week 3 to week 12 postnatal. The waveform patterns and amplitudes of ERG recording in B6 mice were very stable in either situation (*left column*, **A**, **B**). The amplitude gradually decreased from week 3 to week 12 in rho$^{-/-}$ mice and no obvious a-wave was observed.

measurement for cone function. Study authors found that the response was quite stable in the first 6 weeks postnatal in rho$^{-/-}$ mice, which indicated that these cones might have residual function during this period. But the cone function was entirely lost over time as a consequence of rod cell death. Therefore, a positive change in this response would indicate rescue of cone function and viability.

Study authors revealed a significant positive association between morphological examination (OCT and histological examinations) and physiological response (ERG) in rho$^{-/-}$ mice. This is in accord with a recent study in rd1 and rd10 mice, in which a correlation was found between histological and OCT measurements of retinal thickness.[28] The linear regression indicates the physiological response became smaller while the morphological thickness of ONL became thinner. The significant correlation between OCT examination and b-wave in ERG, either in dark-adapted or light-adapted conditions, indicates that the OCT measurement may in fact be more accurate and reliable than histological examination. Furthermore, the thickness of ONL collected from histological examination was larger than OCT measurement. This is likely induced by the histological procedures employed here. Besides the advantages of OCT, there might be some disadvantage to using OCT for the morphological measurements. OCT is an optical signal acquisition and processing method. It is an interferometric technique and captures micrometer-resolution and 3-D images from within optical scattering media (e.g., biological tissue). Therefore, OCT application strongly depends on the optical properties of the tissue in the visual axis. The different layers of the retina have different refractive indices—for example, the inner segment ellipsoids with rich lipids have higher refraction.[29] These differences will affect the scaling of the OCT signal and the measurements from OCT images.

Study authors also measured the thickness of the inner nuclear layer from the OCT and histological images, and no difference was found between the different time points in rhodopsin$^{-/-}$ mice, and no difference between rhodopsin$^{-/-}$ mice and the wild type B6 mice. It suggests that there is no morphological change in the inner nuclear layer during retinal degeneration in this model.

In conclusion, morphological examination and ERG recording confirmed that the application of OCT is able to yield accurate and reliable measurements of ONL thickness. Therefore, SD-OCT can be a reliable, noninvasive way to monitor the dynamic changes in retina degenerative animal models, and this developing technique also shows great potential in further evaluation of interventional strategies.

This is the first study to report the dynamic changes in the retina of rhodopsin$^{-/-}$ mice using SD-OCT. Study findings confirmed that SD-OCT is able to yield accurate and reliable results, which will significantly contribute to the further studies in this field.

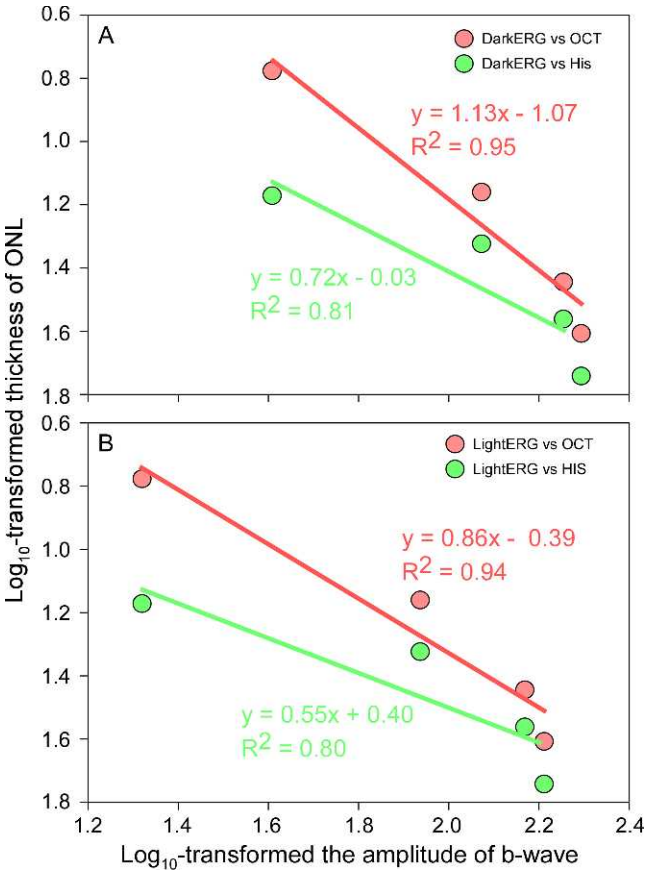

Figure 6. The relationships between morphological and functional changes in rho$^{-/-}$ mice. Significant positive associations were yielded between the thickness of ONL and the ERG recording, either in dark-adapted (**A**) or in light-adapted situation (**B**). All of the data were normalized for yielding the associations by $\log_{10}$-transformation.

Acknowledgments

The authors thank Prof. Peter Humphries for kindly providing rhodopsin$^{-/-}$ mice.

References

1. Hartong DT, Berson EL, Dryja TP. Retinitis pigmentosa. *The Lancet*. 2006;368:1795–1809.
2. Amresh C, Usha C, Dinesh V. Age related macular degeneration. *BMJ*. 2003;326:485–488.
3. O'Shea JG. Age-related macular degeneration. *Postgrad Med J*. 1998;74:203–207.
4. Hargravz PA, McDowell JH. Rhodopsin and phototransduction: a model system for G protein-linked receptors. *FASEB J*. 1992; 6:2323–2331.
5. Schertler GFX. Structure of rhodopsin. *Eye*. 1998;12:504–510.
6. Humphries MM, Rancourt D, Farrar GJ, et al. Retinopathy induced in mice by targeted disruption of the rhodopsin gene. *Nat Genet*. 1997;15:216–219.
7. Toda K, Bush RA, Humphries P, Sieving PA. The electroretinogram of the rhodopsin knockout mouse. *Vis Neurosci*. 1999; 16:391–398.
8. Jaissle GB, May CA, Reinhard J, et al. Evaluation of the rhodopsin knockout mouse as a model of pure cone function. *Invest Ophthalmol Vis Sci*. 2001;42:506–513.
9. Smith L, MacNeil S. State of the art in non-invasive imaging of cutaneous melanoma. *Skin Res Technol*. 2011;17:257–269.
10. Klassen H, Sakaguchi DS, Young MJ. Stem cells and retinal repair. *Prog Retin Eye Res*. 2004;23:149–181.
11. MacLaren RE, Pearson RA, MacNeil A, et al. Retinal repair by transplantation of photoreceptor precursors. *Nature*. 2006; 444:203–207.
12. Tucker BA, Park I-H, Qi SD, et al. Transplantation of adult mouse iPS cell-derived photoreceptor precursors restores retinal structure and function in degenerative mice. *PLoS ONE*. 2011;6:e18992.
13. Yao J, Tucker BA, Zhang X, Checa-Casalengua P, Herrero-Vanrell R, Young MJ. Robust cell integration from co-transplantation of biodegradable MMP2-PLGA microspheres with retinal progenitor cells. *Biomaterials*. 2011;32:1041–1050.
14. Huber G, Beck SC, Grimm C, et al. Spectral domain optical coherence tomography in mouse models of retinal degeneration. *Invest Ophthalmol Vis Sci*. 2009;50:5888–5895.
15. Drexler W, Fujimoto JG. State-of-the-art retinal optical coherence tomography. *Prog Retin Eye Res*. 2008;27:45–88.
16. Puliafito C, Hee M, Lin C, et al. Imaging of macular diseases with optical coherence tomography. *Ophthalmology*. 1995; 102:217–229.
17. Bowd C, Zangwill LM, Berry CC, et al. Detecting early glaucoma by assessment of retinal nerve fiber layer thickness and visual function. *Invest Ophthalmol Vis Sci*. 2001;42:1993–2003.
18. Srinivasan VJ, Adler DC, Chen Y, et al. Ultrahigh-speed optical coherence tomography for three-dimensional and en face Imaging of the retina and optic nerve head. *Invest Ophthalmol Vis Sci*. 2008;49:5103–5110.
19. Gabriele ML, Wollstein G, Ishikawa H, et al. Optical coherence tomography: history, current status, and laboratory work. *Invest Ophthalmol Vis Sci*. 2011;52:2425–2436.
20. Huang D, Swanson E, Lin C, et al. Optical coherence tomography. *Science*. 1991;254:1178–1181.
21. Swanson E, Izatt J, Hee M, et al. In vivo retinal imaging by optical coherence tomography. *Opt Lett*. 1993;18:1864–1866.
22. Fercher A, Hitzenberger C, Drexler W, Kamp G, Sattmann H. In vivo optical coherence tomography. *Am J Ophthalmol*. 1993; 116:113–114.
23. Li Q, Timmers AM, Hunter K, et al. Noninvasive imaging by optical coherence tomography to monitor retinal degeneration in the mouse. *Invest Ophthalmol Vis Sci*. 2001;42:2981–2989.
24. Ruggeri M, Wehbe H, Jiao S, et al. In vivo three-dimensional high-resolution imaging of rodent retina with spectral-domain optical coherence tomography. *Invest Ophthalmol Vis Sci*. 2007;48:1808–1814.
25. Kim KH, Puoris'haag M, Maguluri GN, et al. Monitoring mouse retinal degeneration with high-resolution spectral-domain optical coherence tomography. *J Vis*. 2008;817;11–11.
26. Fischer MD, Huber G, Beck SC, et al. Noninvasive, in vivo assessment of mouse retinal structure using optical coherence tomography. *PLoS ONE*. 2009;4:e7507.
27. Marmor M, Fulton A, Holder G, Miyake Y, Brigell M, Bach MISCEV. Standard for full-field clinical electroretinography (2008 update). *Doc Ophthalmol*. 2009;118:69–77.
28. Pennesi ME, Michaels KV, Magee SS, et al. Long-term characterization of retinal degeneration in rd1 and rd10 mice using spectral domain optical coherence tomography [published online ahead of print May 3, 2012]. *Invest Ophthalmol Vis Sci*. doi:10.1167/iovs.12-9611.
29. Sidman RL. The structure and concentration of solids in photoreceptor cells studied by refractometry and interference microscopy. *J Biophys Biochem Cytol*. 1957;3:15–30.